FINITE DIFFERENCE MODEL FOR THE BUCKLING ANALYSIS OF SANDWICH PIPES UNDER EXTERNAL PRESSURE

by Rouzbeh Hashemian[(a)] and Magdi Mohareb[(a)*]

[(a)] Department of Civil Engineering, University of Ottawa, Ottawa, ON, K1N 6N5

Abstract

A general eigenvalue buckling solution is developed for the buckling of sandwich pipes with thick cores subjected to internal and external hydrostatic pressure. The formulation accounts for shear deformation effects and involves two destabilizing terms: one is due to the external hydrostatic pressure and incorporates the follower effects, and the other, is due to the pre-bucking stresses undergoing the nonlinear components of strains. Work conjugate triplets consisting the Cauchy stress tensor, the Green-Lagrange strain tensor, and constant constitutive relations are adopted in the formulation. The principle of stationary potential energy is used to formulate the conditions of equilibrium and neutral stability conditions using polar coordinates. A finite difference solution is developed and implemented in MATLAB and then applied to predict the buckling capacity of sandwich pipes consisting of two steel pipes with a soft core. A comprehensive verification study is conducted, and the validity of the formulation is established through comparison with other solutions. A parametric study is then carried out to investigate the effect of internal pressure, the thickness and material properties of the core, internal and external pipe thicknesses, on the buckling of sandwich pipes. Simple design equations are developed to predict the critical pressure of sandwich pipes.

Keywords

Sandwich pipes, External pressure, Buckling, Eigenvalue analysis, Finite difference, Polar coordinates, simplified design equations.

This article is to be cited as
Hashemian R., Mohareb M, (2016), Finite difference model for the buckling analysis of sandwich pipes under external pressure, Ocean Engineering, 122, 172-185

The copy-edited version of this article is available at https://doi.org/10.1016/j.oceaneng.2016.06.003

*Corresponding author. Tel. +1 (613) 562 5800 x 6130, fax +1 (613) 563 5173
Email Address: mmohareb@uottawa.ca (M. Mohareb)

1 Introduction

Sandwich pipes consist of an internal steel pipe, a core layer made from a relatively softer material, and external steel pipe. With the continuous search for oil and gas at deep subsea depths, offshore pipelines are being built at depths of more than 2000 m. In such situations involving high external pressure, conventional engineering solutions involving thick steel pipes can become uneconomic when compared to sandwich pipe systems. Within this context, the present study develops an accurate and efficient finite difference solution for the buckling analysis of sandwich pipes under the effect of external pressure and internal pressure.

2 Literature Review

The present study aims at developing a buckling solution for sandwich pipe system consisting of multiple layers and subjected to internal and external pressure. Since sandwich systems involve a thick core, buckling solutions of thick pipes are first reviewed in Section 2.1 and then buckling solutions for sandwich pipe systems are reviewed in Section 2.2.

2.1 Thick Pipes under External Pressure

Studies on the buckling of rings include the work of Kardomateas (1993) who developed an elasticity solution for the buckling of orthotropic cylindrical thick shells. Fu and Waas (1995) developed a shear deformable model for the buckling of pipes and a 2D formulation based on a variational approach. By considering the destabilizing effect induced by stresses undergoing non-linear strains, Papadakis (2008) developed a buckling solution for thick pipes. Most recently, Ji and Waas (2013) formulated an energy conjugate 2D elasticity solution based on the Jaumann rate of Kirchhoff stress tensor, the Green-Lagrange Strain tensor, and a constant constitutive tensor.

2.2 Sandwich Pipes under External Pressure

Based on a ring on elastic foundation analogy, Brush and Almroth (1975) developed an approximate buckling solution for sandwich pipes. By incorporating shear deformation effects, Kardomateas and Simitses (2004) developed a 3D buckling solution for sandwich cylindrical shells subjected to external pressure. Sato and Patel (2007) investigated the elastic buckling pressure of sandwich pipes involving two thin pipes with thick core layer. Their solution neglects the non-linear components of the strain-displacement relations for the core, and the classical Airy stress function approach was thus used to characterize the stresses within the core. Within this context, the present study avoids this simplifying assumption by retaining the nonlinear strain-displacement components. Arjomandi and Taheri (2010) developed an analytical solution for the buckling pressure of sandwich pipes for various bonding conditions at the pipe-core interfaces, namely; a) full bond to with inner and outer pipes, b) unbonded from the outer pipe, but fully bonded to the inner pipe, c) unbonded to the inner pipe, but fully bonded to the outer pipe, and d) unbonded from both the inner and outer pipes.

In contrast to other solutions on sandwich pipes, the present study adopts energy conjugate stress-strain-constitutive parameters in a manner similar to Ji and Waas (2013), accounts for shear deformation effects in the steel pipes, and captures the destabilizing effect of pre-buckling stresses undergoing non-linear strains. Similar to the studies of Sato and Patel (2007), Arjomandi and Taheri (2011), the present study accounts for shear deformation effects within the core, and for the presence of internal pressure. Fu et al. (2014) experimentally investigated the collapse propagation of sandwich pipes. Their 2D FEA model in ABAQUS has shown good agreement with their experimental results.

3 Statement of the Problem

A sandwich pipe system is assumed to involve l layers with different materials (Figure 1). Each layer $j = 1, 2, 3, \ldots l$ has an internal radius r_{j-1} and an external radius r_j, and a thickness $d_j = r_j - r_{j-1}$ (Figure 1(a)). The pipe is subjected to an internal hydrostatic pressure P_{int} acting on the inside radius r_0 and an external hydrostatic pressure P_{ext} acting on the outside radius r_l. Sign conventions of both pressures are shown in Figure 1(b). It is required to determine the external pressure P_{ext} that induces buckling of the sandwich system.

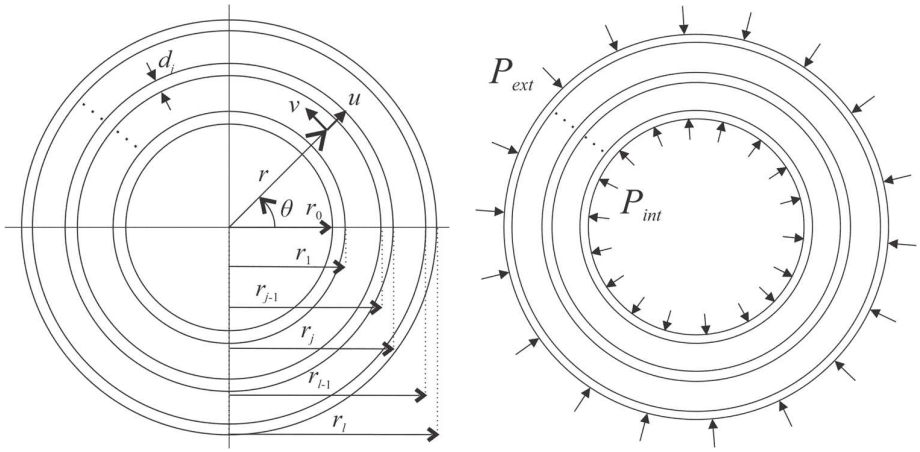

(a) (b)

Figure 1. Sandwich Pipe System (a) Notation, (b) Positive sign conventions for internal and external pressure

4 Assumptions

The main assumptions of the formulation are:

(i) The sandwich pipe system is assumed to be long. As such, it is idealized as a plane strain problem,

(ii) Each layer is assumed to be linearly elastic and isotropic

(iii) Both internal and external pressures are assumed to remain normal to the deformed pipe surface, i.e., the follower effect is to be captured by the model,

(iv) Full bonding is assumed between all layers of the composite pipe system, and

(v) The formulation neglects the initial geometric imperfections of the system and thus predicts the critical pressure through an eigenvalue analysis.

5 Formulation

5.1 Kinematics and Notation

A polar coordinates system (r,θ) is adopted (Figure 1a). For layer j, displacement u^j defined along the radial direction and displacement v^j defined along the tangential direction are functions of coordinates r and θ. Configuration (a) in Figure 2 depicts the initial configuration of the composite system prior to loading. An internal pressure P_{int} is then applied to the inside surface. Under the applied pressure, the system is assumed to undergo a radial pre-buckling displacements $u_{pI}^j(r)$ as depicted by Configuration (b). An external pressure P_{ext} is then applied to the outer surface of the system. The system then deforms as per Configuration (c). The additional displacement associated with the external pressure is characterized by the pre-buckling displacement $-u_{pE}^j(r)$ and is to be added to the pre-buckling displacement field u_{pI}^j. Thus, the radial displacement at Configuration (c) is $u_{pI}^j - u_{pE}^j$. As a matter of convention, displacement u_{pE} is taken positive in the outward direction, in a manner that is consistent with the sign convention of the radial coordinate r. The external pressure is assumed to increase until the pipe attains the state of onset of buckling at an external pressure λP_{ext} as depicted in Configuration (d). The displacement associated with configuration (d) becomes $u_{pI}^j - \lambda u_{pE}^j$, in which λ is the load/displacement multiplier sought. Throughout buckling, hydrostatic pressures P_{int} and λP_{ext} are assumed to remain constant and the system is assumed to deform from Configuration (d) to Configuration (e). The additional buckling displacements are the

radial displacements u_b^j and tangential displacements v_b^j. The final displacements at Configuration (e) are obtained by adding the displacement fields at the onset of buckling to those during buckling, i.e.,

$$\begin{aligned} u^j &= u_{pI}^j - \lambda u_{pE}^j + u_b^j, \\ v^j &= 0 + v_b^j \end{aligned} \tag{1}$$

As a matter of convention, all displacement fields induced throughout the pre-buckling are indicated by a subscript *p* while all those arising during buckling are denoted by subscript *b*. The notation is further extended in the following sections to other fields such as strains and stresses.

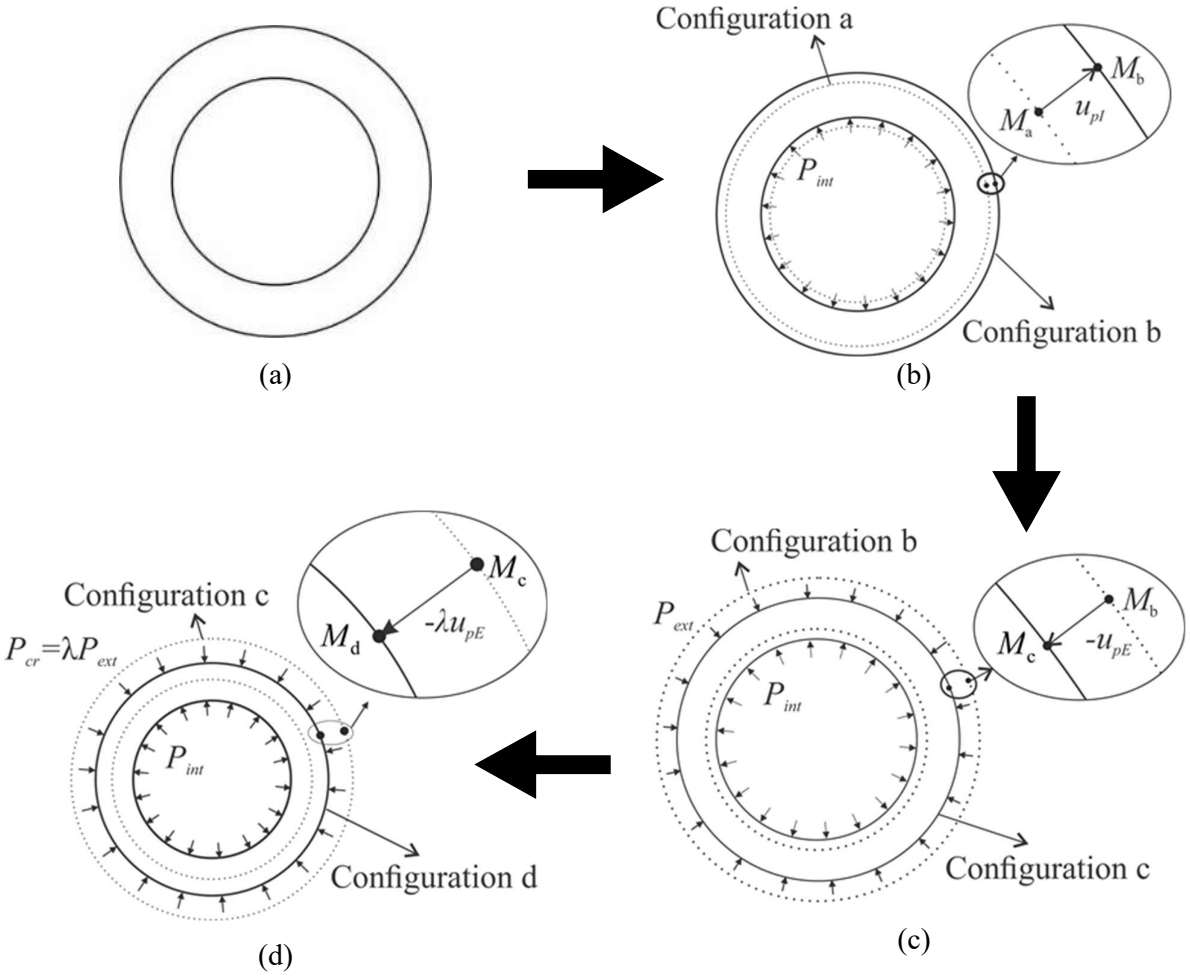

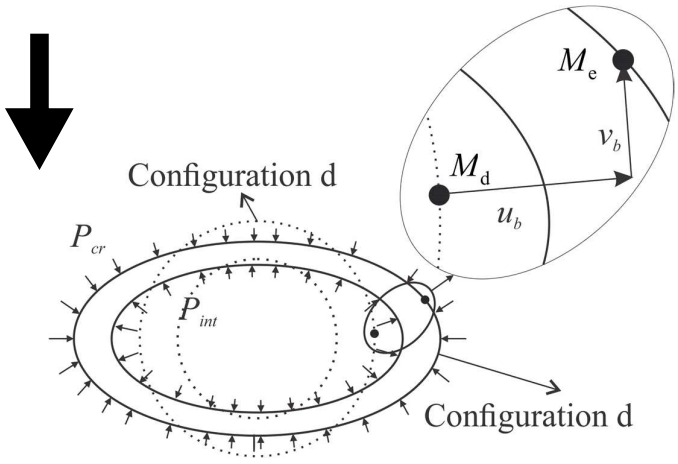

(e)

Figure 2. Pipe Kinematics (a) undeformed, (b) pre-buckling under internal pressure, (c) pre-buckling under internal and reference external pressure, (d) at the onset of buckling, and (e) buckled configuration

5.2 Strain-Displacement Relationship

The 2D Green-Lagrange strain displacement relations in polar coordinates (e.g.,Kardomateas (1993)) are

$$\begin{aligned}
\varepsilon_r^j &= u'^j + \frac{1}{2}\left(u'^{j2} + v'^{j2}\right) \\
\varepsilon_\theta^j &= \frac{1}{r}\left(u^j + \dot{v}^j\right) + \frac{1}{2r^2}\left[\dot{u}^{j2} + v^{j2} - 2\dot{u}^j v^j + u^{j2} + \dot{v}^{j2} + 2u^j\dot{v}^j\right] \\
\gamma_{r\theta}^j &= \frac{1}{r}\left(\dot{u}^j - v^j\right) + v'^j + \frac{1}{r}\left(\dot{u}^j u'^j - u'^j v^j + u^j v'^j + v'^j\dot{v}^j\right)
\end{aligned} \tag{2}$$

where all primes denote differentiation with respect to the radial coordinate r and dots denote differentiation of with respect to coordinate θ.

5.3 Strain Decomposition

The strains are expressed in terms of the pre-buckling and buckling displacements by substituting Eqs. (1) into Eqs. (2). The strain terms are divided into linear and nonlinear components (Appendix-1). As a convention, all the linear strains are denoted with subscript L while the non-linear strains are

denoted with subscript *NL*. According to this notation, each of the total strains (i.e., going from Configuration (a) to (d) has four components, i.e.,

$$\begin{aligned}
\varepsilon_r{}^j &= \varepsilon^j_{r,L,p} + \varepsilon^j_{r,NL,p} + \varepsilon^j_{r,L,b} + \varepsilon^j_{r,NL,b} \\
\varepsilon_\theta{}^j &= \varepsilon^j_{\theta,L,p} + \varepsilon^j_{\theta,NL,p} + \varepsilon^j_{\theta,L,b} + \varepsilon^j_{\theta,NL,b} \\
\gamma_{r\theta}{}^j &= \gamma^j_{r\theta,L,p} + \gamma^j_{r\theta,NL,p} + \gamma^j_{r\theta,L,b} + \gamma^j_{r\theta,NL,b}
\end{aligned} \tag{3}$$

and ε_r^j is the total radial strain ε_θ^j is the total tangential strain and $\gamma_{r\theta}^j$ is the total shear strain. Expressions for the components of Eq. (3) are given in Appendix A. For a sandwich pipe system consisting of l layers $j = 1, 2, ...l$, the total potential energy Π is given by

$$\Pi = \sum_{j=1}^{l} U^j + W_1 + W_2 \tag{4}$$

where the internal strain energy term is the summation of all layers U^j and W_1 and W_2 are load potential gained by the internal and external pressures respectively. The internal strain energy U_j for a single layer (e.g., Brush and Almroth 1975) is

$$U^j = \frac{L^j}{2\upsilon^j} \int_{r_0}^{r_j} \int_0^{2\pi} \left[\left(1-\upsilon^j\right)(\varepsilon_r^{j2} + \varepsilon_\theta^{j2}) + 2\upsilon^j \varepsilon_r^j \varepsilon_\theta^j + \frac{1-2\upsilon^j}{2} \gamma_{r\theta}^{j\,2} \right] r d\theta dr \tag{5}$$

Also, the destabilizing terms due to the internal and external pressure (e.g., Pearson (1955) are

$$\begin{aligned}
W_1 &= -P_{int} \int_0^{2\pi} \left[u^j r + \frac{1}{2}\left(v^{j2} + u^{j2} - v^j \dot{u}^j + \dot{v}^j u^j\right) \right]_{r_0} d\theta, \qquad j = 1 \\
W_2 &= \lambda P_{ext} \int_0^{2\pi} \left[u^j r + \frac{1}{2}\left(v^{j2} + u^{j2} - v^j \dot{u}^j + \dot{v}^j u^j\right) \right]_{r_l} d\theta, \qquad j = l
\end{aligned} \tag{6}$$

In Eqs. (5) and (6), $L^j = E^j \upsilon^j / (1+\upsilon^j)(1-2\upsilon^j)$ is the Lame's constant and υ^j is the Poisson's ratio for Layer *j*.

5.4 Pre-Buckling Analysis

Configurations (b)-(d) of the pipe system in Figure 2 are determined from pre-buckling equilibrium considerations. The corresponding total potential energy expression Π_p is obtained by omitting the buckling displacements, and setting the variation of Π_p to zero, yielding

$$\begin{aligned}\overline{\Pi}_p = \sum_{j=1}^{l}\left\{\int_{r_{j-1}}^{r_j}\int_0^{2\pi}\frac{L^j}{2\upsilon^j}\left[\left(1-\upsilon^j\right)\left(2ru_p'^j\overline{u}_p'^j+2\frac{1}{r}u_p^j\overline{u}_p^j\right)+2\upsilon^j u_p^j\overline{u}_p'^j+2\upsilon^j u_p'^j\overline{u}_p^j\right]d\theta dr\right\} \\ +\lambda P_{ext}\int_0^{2\pi}\left(r\overline{u}_p^l\right)_{r_l}d\theta-P_{int}\int_0^{2\pi}\left(r\overline{u}_p^1\right)_{r_0}d\theta=0\end{aligned} \tag{7}$$

where $\overline{(\,)}$ denotes the first variation of the argument function and $u_p^j(\lambda)$ is the pre-buckling displacement of Layer *j* due to the external and internal pressure and depends on the value of λ. The pre-buckling displacements at Configurations (b), (c), and (d), are respectively denoted by $u_p^j(\lambda=0)$, $u_p^j(\lambda=1)$, and $u_p^j(\lambda)$. Note that the $u_p^j(\lambda=0)$ is associated with the pre-buckling displacement due to the internal pressure alone, i.e., $u_{pI}^j=u_p^j(\lambda=0)$ and the pre-buckling displacement u_{pE}^j due to the external pressure alone is $u_{pE}^j=u_p^j(\lambda=1)-u_p^j(\lambda=0)$.

The nonlinear strain components are neglected in the pre-buckling analysis. This assumption is justified as long as the system is relatively rigid, as is the case herein where the presence of steel pipes ensures small pre-buckling displacements within the system. By performing integration by parts on Eq. (7) and grouping like terms, one recovers *l* equilibrium equations associated with the layers of the sandwich pipe systems of the form $\frac{1}{r}u_p^j(\lambda)-u_p'^j(\lambda)-ru_p''^j(\lambda)=0$ where $r_{j-1}\le r\le r_j$ and $j=1,2,\cdots l$. The solution of the above equilibrium equations takes the form

$$u_p^j(\lambda)=\overline{F}_1^j(\lambda)r+\overline{F}_2^j(\lambda)r^{-1}\qquad r_{j-1}\le r\le r_j \tag{8}$$

where $\bar{F}_1^j(\lambda)$, $\bar{F}_2^j(\lambda)$ ($j=1,2,...l$) are integration constants to be obtained from the boundary conditions and interlayer continuity conditions. The boundary equations at the internal and external surfaces of the system take the form

$$\begin{cases} \left\{-r_0 P_{int} - \left[L^j\left[\left(1-\upsilon^j\right)/\upsilon^j\right] r_0 u_p'^j + L^j u_p^j\right]\right\}\bar{u}_p^j = 0, & j=1 \\ \left\{r_l \lambda P_{ext} + \left[\dfrac{L^j\left(1-\upsilon^j\right)}{\upsilon^j} r_l u_p'^j + L^j u_p^j\right]\right\}\bar{u}_p^j = 0, & j=l \end{cases} \tag{9}$$

By grouping the boundary terms at each of the interlayers, one recovers $l-1$ continuity equations

$$\left\{\left[\frac{\left(1-\upsilon^j\right)}{\upsilon^j} L^j r_j u_p'^j\left(r_j\right) + L^j u_p^j\left(r_j\right)\right] - \left[\frac{\left(1-\upsilon^{j+1}\right)}{\upsilon^{j+1}} L^{j+1} r_j u_p'^{j+1}\left(r_j\right) + L^{j+1} u_p^{j+1}\left(r_j\right)\right]\right\}\bar{u}_p^j\left(r_j\right) = 0 \tag{10}$$

5.5 Buckling Analysis

The second variation of the total potential energy is given by (Hashemian and Mohareb 2015)

$$\begin{aligned} \frac{1}{2}\overline{\overline{\Pi}} = \sum_{j=1}^{l}\Bigg\{ & \int_{r_{j-1}}^{r_j}\int_0^{2\pi} \frac{L^j\left(1-\upsilon^j\right)}{2\upsilon^j}\left[r\left(\bar{u}'^j_b\right)^2 + \frac{1}{r}\left(\bar{u}^j_b + \dot{\bar{v}}^j_b\right)^2\right] + L^j \bar{u}'^j_b\left(\bar{u}^j_b + \dot{\bar{v}}^j_b\right) \\ & + \frac{L^j\left(1-\upsilon^j\right)}{2\upsilon^j}\underline{\underline{\left[\left(u^j_{p,I} + \lambda u^j_{p,E}\right)\left(\bar{u}'^{j2}_b + \bar{v}'^{j2}_b\right) + r\left(u'^j_{p,I} + \lambda u'^j_{p,E}\right)\left(\bar{u}'^{j2}_b + \bar{v}'^{j2}_b\right)\right]}} \\ & + \frac{L^j(1-2\upsilon^j)}{4\upsilon^j} r\left(\frac{1}{r}\dot{\bar{u}}^j_b - \frac{1}{r}\bar{v}^j_b + \bar{v}'^j_b\right)^2 + \frac{1}{2}L^j\underline{\underline{\left[\left(u^j_{p,I} + \lambda u^j_{p,E}\right)\left(\bar{u}'^{j2}_b + \bar{v}'^{j2}_b\right)\right.}} \\ & \underline{\underline{\left. + \frac{1}{r}\left(u'^j_{p,I} + \lambda u'^j_{p,E}\right)\left(\dot{\bar{u}}^{j2}_b + \bar{v}^{j2}_b - 2\dot{\bar{u}}^j_b\bar{v}^j_b + \bar{u}^{j2}_b + \dot{\bar{v}}^{j2}_b + 2\bar{u}^j_b\dot{\bar{v}}^j_b\right)\right]}}\Bigg\} d\theta dr \\ & - \frac{1}{2}P_{int}\int_0^{2\pi}\left[\left(\bar{v}^j_b\right)^2 + \left(\bar{u}^j_b\right)^2 - \bar{v}^j_b\dot{\bar{u}}^j_b + \dot{\bar{v}}^j_b\bar{u}^j_b\right]_{r_0} d\theta + \underline{\frac{1}{2}\lambda P_{ext}\int_0^{2\pi}\left[\left(\bar{v}^j_b\right)^2 + \left(\bar{u}^j_b\right)^2 - \bar{v}^j_b\dot{\bar{u}}^j_b + \dot{\bar{v}}^j_b\bar{u}^j_b\right]_{r_l} d\theta} \end{aligned} \tag{11}$$

where $\overline{\overline{(\,)}}$ denotes the second variation of the argument functions (or functional). It is noted that the destabilizing term underlined by a single line has been considered in past sandwich pipe studies (e.g.,

Sato and Patel (2007)), while the additional destabilizing terms underlined with double lines result from retaining the non-linear terms in the present study. The variation of the displacements $\bar{u}_b$ and $\bar{v}_b$ are functions of r and θ. Given their harmonic nature in coordinate θ, they can be expressed as

$$\bar{u}_b^j(r,\theta)=\sum_{n=1}^{\alpha} f_n^j(r)\cos n\theta, \qquad \bar{v}_b^j(r,\theta)=\sum_{n=1}^{\alpha} g_n^j(r)\sin n\theta \tag{12}$$

where $r_{j-1}\le r\le r_j$ and Eqs. (12) converge to the exact solution as $\alpha\to\infty$. For practical purposes, a finite number of terms α is taken. From Eqs. (12), by substituting into Eq. (11), taking advantage of the orthogonality conditions

$$\begin{aligned}
&\int_{\theta=0}^{2\pi}\sum_{m}^{\alpha}\sum_{n=1}^{\alpha} f_n(r)\,g_m(r)\cos n\theta\sin m\theta d\theta=0\\
&\int_{\theta=0}^{2\pi}\sum_{m}^{\alpha}\sum_{n=1}^{\alpha} f_n(r)\,g_m(r)\sin n\theta\sin m\theta d\theta=\sum_{n=1}^{\alpha}2\pi f_n(r)\,g_n(r)
\end{aligned} \tag{13}$$

and integrating Eq. (11) with respect θ, one obtains

$$\begin{aligned}
\frac{1}{2}\overline{\overline{\Pi}}=\sum_{j=1}^{l}\sum_{n=1}^{\alpha}2\pi\int_{r_{j-1}}^{r_j}\Bigg\{&\frac{L^j\left(1-\upsilon^j\right)}{2\upsilon^j}\left[r\left(f_n'^j\right)^2+\frac{1}{r}\left(f_n^j+ng_b^j\right)^2\right]+L^j f_n'^j\left(f_n^j+ng_b^j\right)\\
&+\frac{L^j\left(1-\upsilon^j\right)}{2\upsilon^j}\left(u_{p,I}+\lambda_n u_{p,E}\right)\left[\left(f_n'^j\right)^2+\left(g_n'^j\right)^2\right]+\frac{L^j\left(1-\upsilon^j\right)}{2\upsilon^j}r\left(u_{p,I}'^j+\lambda_n u_{p,E}'^j\right)\left[\left(f_n'^j\right)^2+\left(g_n'^j\right)^2\right]\\
&+\frac{L^j(1-2\upsilon^j)}{4\upsilon^j}r\left(\frac{1}{r}nf_n^j-\frac{1}{r}g_n^j+g_n'^j\right)^2+\frac{1}{2}L^j\left[\left(u_{p,I}^j+\lambda_n u_{p,E}^j\right)\left[\left(f_n'^j\right)^2+\left(g_n'^j\right)^2\right]\right.\\
&\left.+\frac{1}{r}\left(u_{p,I}'^j+\lambda_n u_{p,E}'^j\right)\left[\left(-nf_n^j\right)^2+\left(g_n^j\right)^2+\left(f_n^j\right)^2+\left(ng_n^j\right)^2+4nf_n^j g_n^j\right]\right\}dr\\
&-\pi P_{int}\left[\left(g_n^j\right)^2+\left(f_n^j\right)^2+ng_n^j f_n^j+ng_n^j f_n^j\right]_{r_0}+\pi\lambda_n P_{ext}\left[\left(g_n^j\right)^2+\left(f_n^j\right)^2+2ng_n^j f_n^j\right]_{r_l}
\end{aligned} \tag{14}$$

It is clear that the functions f_n^j, g_n^j and their derivatives appearing in Eq. 14 do not depend on the circumferential coordinate, transforming the 2D problem into a series of 1D problem. The conditions of neutral stability conditions are obtained by setting the variation of the second variation of the total

potential energy to zero, i.e., $\delta(1/2\,\overline{\overline{\Pi}})=0$. By performing integration by parts, one recovers $2(n-1)\times l$ field equations of the form

$$\int_{r_{j-1}}^{r_j}\Big[\Big(A_{1,1}^j f_n^j + A_{1,2}^j f_n'^j + A_{1,3}^j f_n''^j - A_{1,4}^j n^2 f_n^j + A_{1,5}^j n g_n^j + A_{1,6}^j n g_n'^j\Big) + \lambda_n\Big(B_{1,1}^j f_n^j + B_{1,2}^j f_n'^j + B_{1,3}^j f_n''^j - B_{1,4}^j n^2 f_n^j + B_{1,5}^j n g_n^j\Big)\Big]\delta f_n^j dr = 0 \tag{15}$$

$$\int_{r_{j-1}}^{r_j}\Big[\Big(-A_{2,1}^j n f_n^j - A_{2,2}^j n f_n'^j + A_{2,3}^j g_n^j + A_{2,4}^j g_n'^j + A_{2,5}^j g_n''^j - A_{2,6}^j n^2 g_n^j\Big) + \lambda_n\Big(-B_{2,1}^j n f_n^j + B_{2,2}^j g_n^j + B_{2,3}^j g_n'^j + B_{2,4}^j g_n''^j - B_{2,5}^j n^2 g_n^j\Big)\Big]\delta g_n^j dr = 0 \tag{16}$$

where $1\le j\le l$ and $n=2,3,4...,\alpha$ and constants $A_{k,m}^j\,(k=1,2,m=1,...6)$ and $B_{k,m}^j\,(k=1,2,m=1,...5)$ introduced in Equations (15) and (16) are provided in Appendix B. The interlayer continuity equations arise from grouping the boundary terms resulting from integration by parts leading to $(n-1)\times(l-1)$ pairs of equations of the form

$$\Big\langle\Big\{\Big[\Big(C_{3,1}^j f_n^j + C_{3,2}^j f_n'^j + C_{3,3}^j n g_n^j\Big) + \lambda_n\Big(D_{3,2}^j f_n^{j'}\Big)\Big] - \Big[\Big(C_{1,1}^{j+1} f_n^{j+1} + C_{1,2}^{j+1} f_n'^{j+1} + C_{1,3}^{j+1} n g_n^j\Big) + \lambda_n\Big(D_{1,1}^{j+1} f_n'^j\Big)\Big]\Big\}\delta f_n^j\Big\rangle_{r=r_j} = 0 \tag{17}$$

$$\Big\langle\Big\{\Big[\Big(-C_{4,1}^j n f_n^j + C_{4,2}^j g_n^j + C_{4,3}^j g_n'^j\Big) + \lambda_n\Big(D_{4,3}^j g_n'^j\Big)\Big] - \Big[\Big(-C_{2,1}^{j+1} n f_n^{j+1} + C_{2,2}^{j+1} g_n^{j+1} + C_{2,2}^{j+1} g_{n\,n}'^{j+!}\Big) + \lambda_n\Big(D_{2,1}^{j+1} g_n'^{j+!}\Big)\Big]\Big\}\delta g_n^j\Big\rangle_{r=r_j} = 0 \tag{18}$$

where $1\le j\le l-1$. The boundary equations at the inside boundary are

$$\Big\{\Big[C_{1,1}^1 f_n^1 + C_{1,2}^1 f_n'^1 + C_{1,3}^1 n g_n^1 + \lambda_n\Big(D_{1,1}^1 f_n'^1\Big)\Big]\delta f_n^1\Big\}_{r=r_0} = 0 \tag{19}$$

$$\Big\{\Big[\Big(-C_{2,1}^1 n f_n^1 + C_{2,2}^1 g_n^1 + C_{2,3}^1 g_n'^1\Big) + \lambda_n\Big(D_{2,1}^1 g_n'^1\Big)\Big]\delta f_n^1\Big\}_{r=r_0} = 0 \tag{20}$$

and those at the outside boundary are

$$\left\{\left[\left(C_{3,1}^{l}f_{n}^{l}+C_{3,2}^{l}f_{n}^{\prime l}+C_{3,3}^{l}ng_{n}^{l}\right)+\lambda_{n}\left(D_{3,1}^{l}f_{n}^{l}+D_{3,2}^{l}f_{n}^{\prime l}+D_{3,3}^{l}ng_{n}^{l}\right)\right]\delta f_{n}^{l}\right\}_{r=r_{l}}=0 \tag{21}$$

$$\left\{\left[\left(-C_{4,1}^{l}nf_{n}^{l}+C_{4,2}^{l}g_{n}^{l}+C_{4,3}^{l}g_{n}^{\prime l}\right)+\lambda_{n}\left(-D_{4,1}^{l}nf_{n}^{l}+D_{4,2}^{l}g_{n}^{l}+D_{4,3}^{l}g_{n}^{\prime l}\right)\right]\delta g_{n}\right\}_{r=r_{l}}=0 \tag{22}$$

where $n=2,3,4...,\alpha$. Constants $C_{k,m}^{j}\left(k=1,...4,m=1,2,3\right)$ and $D_{k,m}^{j}\left(k=1,...4,\ m=1,2,3\right)$ introduced in Eqs. 17-22, have been defined in Appendix B.

6 Finite Difference Solution

Using the central finite difference approximations, Eqs. (15) and (16) are expressed in the a discretized form as

$$\begin{aligned}&\left(-\frac{A_{1,2}^{j}}{2\Delta_{j}}+\frac{A_{1,3}^{j}}{\Delta_{j}^{2}}\right)f_{i-1}^{j}-\frac{A_{1,6}^{j}n}{2\Delta_{j}}g_{i-1}^{j}+\left(A_{1,1}^{j}-\frac{2A_{1,3}^{j}}{\Delta_{j}^{2}}-A_{1,4}^{j}n^{2}\right)f_{i}^{j}+A_{1,5}^{j}ng_{i}^{j}+\left(\frac{A_{1,2}^{j}}{2\Delta_{j}}+\frac{A_{1,3}^{j}}{\Delta_{j}^{2}}\right)f_{i+1}^{j}\\&+\frac{A_{1,6}^{j}n}{2\Delta_{j}}g_{i+1}^{j}+\lambda_{n}\left[\left(-\frac{B_{1,2}^{j}}{2\Delta_{j}}+\frac{B_{1,3}^{j}}{\Delta_{j}^{2}}\right)f_{i-1}^{j}+\left(B_{1,1}^{j}-\frac{2B_{1,3}^{j}}{\Delta_{j}^{2}}-B_{1,4}^{j}n^{2}\right)f_{i}^{j}+B_{1,5}^{j}ng_{i}^{j}+\left(\frac{B_{1,2}^{j}}{2\Delta_{j}}+\frac{B_{1,3}^{j}}{\Delta_{j}^{2}}\right)f_{i+1}^{j}\right]=0\end{aligned} \tag{23}$$

$$\begin{aligned}&\frac{A_{2,2}^{j}n}{2\Delta_{j}}f_{i-1}^{j}+\left(-\frac{A_{2,4}^{j}}{2\Delta_{j}}+\frac{A_{2,5}^{j}}{\Delta_{j}^{2}}\right)g_{i-1}^{j}-A_{2,1}^{j}nf_{i}^{j}+\left(A_{2,3}^{i}-\frac{2A_{2,5}^{i}}{\Delta_{j}^{2}}-A_{2,6}^{i}n^{2}\right)g_{i}^{j}-\frac{A_{2,2}^{j}n}{2\Delta_{j}}f_{i+1}^{j}+\left(\frac{A_{2,4}^{j}}{2\Delta_{j}}+\frac{A_{2,5}^{j}}{\Delta_{j}^{2}}\right)g_{i+1}^{j}\\&+\lambda_{n}\left[\left(-\frac{B_{2,3}^{j}}{2\Delta_{j}}+\frac{B_{2,4}^{j}}{\Delta_{j}^{2}}\right)g_{i-1}^{j}-B_{2,1}^{j}nf_{i}^{j}+\left(B_{2,2}^{j}-\frac{2B_{2,4}^{j}}{\Delta_{j}^{2}}-B_{2,5}^{j}n^{2}\right)g_{i}^{j}+\left(\frac{B_{2,3}^{j}}{2\Delta_{j}}+\frac{B_{2,4}^{j}}{\Delta_{j}^{2}}\right)g_{i+1}^{j}\right]=0\end{aligned} \tag{24}$$

where Δ_{j} is the length of each subdivision within layer j (Figure 3). One recalls that the Eqs. 23 and 24 are for mode *n* and layer *j*. The fact that, in a given equation, *n* is constant is indicative of the fact that the buckling modes are fully uncoupled.

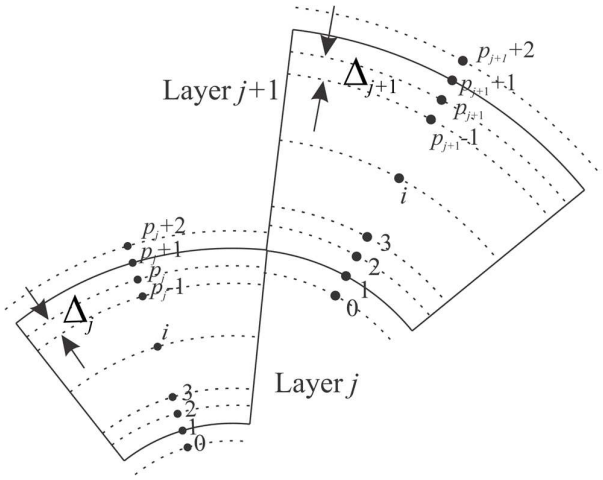

Figure 3. A portion of layers j and j+1 of a sandwich pipe sub-divided into p segments (fictitious nodes at the interlayers are shown)

For mode n, Eqs. (23)-(24) of layer j ($1 \le j \le l$) are applied at each node i = 1… p_j+1, resulting in 2(p_j+1) equations into the 2(p_j+1) unknowns f_1^j, g_1^j, … $f_{p_j+1}^j$, and $g_{p_j+1}^j$. However, when writing the discretized form of the equilibrium equations at nodes $i=1$ and $i=p_j+1$, both lying on the boundaries of the layer j, additional fictitious nodal variables f_0^j, g_0^j, $f_{p_j+2}^j$, $g_{p_j+2}^j$ arise. Thus, the 2(p_j+1) equations include 2(p_j+3) unknowns. The additional equations are obtained by writing the continuity equations and boundary conditions (Eqs. (17) - (22)) in a discretized form. The interlayer continuity equations are expressed as

$$\left(-\frac{C_{3,2}^j}{2\Delta_j}f_p^j + C_{3,1}^j f_{p+1}^j + C_{3,3}^j n g_{p+1}^j + \frac{C_{3,2}^j}{2\Delta_j}f_{p+2}^j\right) + \lambda_n\left(-\frac{D_{3,2}^j}{2\Delta_j}f_p^j + D_{3,1}^j f_{p+1}^j + D_{3,3}^j n g_{p+1}^j + \frac{D_{3,2}^j}{2\Delta_j}f_{p+2}^j\right)$$
$$-\left[-\frac{C_{1,2}^{j+1}}{2\Delta_{j+1}}f_0^{j+1} + C_{1,1}^{j+1}f_1^{j+1} + C_{1,3}^{j+1}n g_1^{j+1} + \frac{C_{1,2}^{j+1}}{2\Delta_{j+1}}f_2^{j+1} + \lambda_n\left(-\frac{D_{1,1}^{j+1}}{2\Delta_{j+1}}f_0^{j+1} + \frac{D_{1,1}^{j+1}}{2\Delta_{j+1}}f_2^{j+1}\right)\right] = 0 \quad (25)$$

$$\left(-\frac{C_{4,3}^{j}}{2\Delta_j}g_p^j - C_{4,1}^{j}nf_{p+1}^{j} + C_{4,2}^{j}g_{p+1}^{j} + \frac{C_{4,3}^{j}}{2\Delta_j}g_{p+2}^{j}\right) + \lambda_n\left(-\frac{D_{4,3}^{j}}{2\Delta_j}g_p^j - D_{4,1}^{j}nf_{p+1}^{j} + D_{4,2}^{j}g_{p+1}^{j} + \frac{D_{4,3}^{j}}{2\Delta_j}g_{p+2}^{j}\right)$$
$$-\left[\left(-\frac{C_{2,3}^{j+1}}{2\Delta_{j+1}}g_0^{j+1} - C_{2,1}^{j+1}nf_1^{j+1} + C_{2,2}^{j+1}g_1^{j+1} + \frac{C_{2,3}^{j+1}}{2\Delta_{j+1}}g_2^{j+1}\right) + \lambda_n\left(-\frac{D_{2,1}^{j+1}}{2\Delta_{j+1}}g_0^{j+1} + \frac{D_{2,1}^{j+1}}{2\Delta_{j+1}}g_2^{j+1}\right)\right] = 0 \quad (26)$$

where $1 \le j \le l-1$. In addition, the boundary conditions at the inside boundary are

$$-\frac{C_{1,2}^{1}}{2\Delta_1}f_0^1 + C_{1,1}^{1}f_1^1 + C_{1,3}^{1}ng_1^1 + \frac{C_{1,2}^{1}}{2\Delta_1}f_2^1 + \lambda_n\left(-\frac{D_{1,1}^{1}}{2\Delta_1}f_0^1 + \frac{D_{1,1}^{1}}{2\Delta_1}f_2^1\right) = 0 \quad (27)$$

$$\left(-\frac{C_{2,3}^{1}}{2\Delta_1}g_0^1 - C_{2,1}^{1}nf_1^1 + C_{2,2}^{1}g_1^1 + \frac{C_{2,3}^{1}}{2\Delta_1}g_2^1\right) + \lambda_n\left(-\frac{D_{2,1}^{1}}{2\Delta_1}g_0^1 + \frac{D_{2,1}^{1}}{2\Delta_1}g_2^1\right) = 0 \quad (28)$$

and those at the outside boundary are

$$\left(-\frac{C_{3,2}^{l}}{2\Delta_l}f_p^l + C_{3,1}^{l}f_{p+1}^{l} + C_{3,3}^{l}ng_{p+1}^{l} + \frac{C_{3,2}^{l}}{2\Delta_l}f_{p+2}^{l}\right) + \lambda_n\left(-\frac{D_{3,2}^{l}}{2\Delta_l}f_p^l + D_{3,1}^{l}f_{p+1}^{l} + D_{3,3}^{l}ng_{p+1}^{l} + \frac{D_{3,2}^{l}}{2\Delta_l}f_{p+2}^{l}\right) = 0 \quad (29)$$

$$\left(-\frac{C_{4,3}^{l}}{2\Delta_l}g_p - C_{4,1}^{l}nf_{p+1} + C_{4,2}^{l}g_{p+1} + \frac{C_{4,3}^{l}}{2\Delta_l}g_{p+2}\right) + \lambda_n\left(-\frac{D_{4,3}^{l}}{2\Delta_l}g_p - D_{4,1}^{l}nf_{p+1} + D_{4,2}^{l}g_{p+1} + \frac{D_{4,3}^{l}}{2\Delta_l}g_{p+2}\right) = 0 \quad (30)$$

For a given mode *n*, applying the interlayer continuity requirements $f_{p_j+1}^{j} = f_1^{j+1}$ and $g_{p_j+1}^{j} = g_1^{j+1}$ will provide the additional equations required to solve for the unknown nodal variables. Solving the above systems of equations will result into $\sum_{j=1}^{l} 2\left(p_j+3\right)$ eigenvalues. The smallest critical pressure $\lambda_n P_{ext}$ is extracted and the procedure is repeated for $n = 1, 2...\alpha$. The buckling pressure of the system is the minimum positive critical pressure based on all modes considered, i.e., $P_{cr} = \min\left(\lambda_1, \lambda_2, ...\lambda_\alpha\right) \times P_{ext}$.

7 Results

7.1 Reference Case

The geometry of the reference case is selected to match that reported in Castello and Estefen (2006). All geometric and material parameters are presented in Table 5. The system is assumed to be subjected to zero internal pressure and external pressure P_{ext}. The critical pressure $P_{cr,Ref} = \lambda P_{ext}$ for the reference composite system is sought.

Table 5. Geometrical and material properties of the reference case.

Layer number j	Nominal Diameter (in)	Inside radius(mm) $r_{j-1,Ref}$	Outside radius(mm) $r_{j,Ref}$	thickness(mm) $d_{j,Ref}$	Young Modulus(MPa) $E_{j,Ref}$	Poisson's ratio $\upsilon_{j,Ref}$
1	6.625	77.75	84.15	6.4	200,000	0.30
2	Annular	84.15	103.15	19	200	0.30
3	8.625	103.15	109.55	6.4	200,000	0.30

7.2 Verification of Pre-buckling Analysis

The results based on the pre-buckling solution developed under Section 5.4 are shown in Figure 4. A comparison with Abaqus results for the reference case when P_{ext} = 1 MPa is also provided. The Abaqus solution is based on the CPE8R element that is used to idealize the problem as a plane strain problem. Forty CPE8R elements were taken in the circumferential direction and 12 elements in the radial direction. A mesh sensitivity study has shown that the 40x12 mesh is enough to achieve convergence. The numeric solution is shown to be in excellent agreement with the Abaqus model.

7.3 Verification of Buckling Analysis

7.3.1 Mesh Study

Figure 5 shows a mesh sensitivity analysis for the mode $n = 2$ based on the present solution and the finite element formulation developed in Hashemian (2014). While the present finite difference solution (FD) exhibits slower convergence than the finite element solution (FE), it has the desirable

property of converging to the buckling pressure from below, i.e., discretization errors on the part of the analyst are observed to lead to an underestimation of the critical pressure, thus inducing an error on the conservative side. Convergence is attained by taking 15 subdivisions per layer.

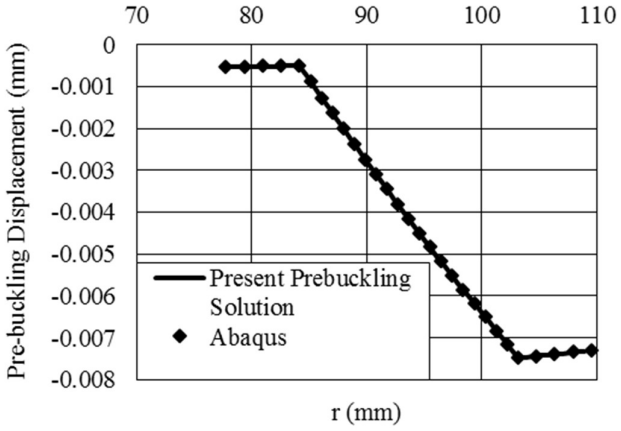

Figure 4. Verification of Pre-buckling solution

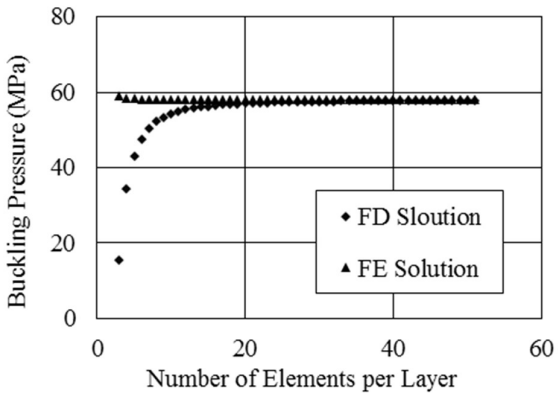

Figure 5. Mesh study

7.3.2 Buckling Pressure and Higher Buckling Modes

The FD buckling solution is used to determine the buckling pressure. Figure 6 represents the buckling pressure of the reference case for various buckling modes n = 2, 3… To each mode n, corresponds a distinct buckling pressure and the critical pressure sought is that corresponding to the smallest value. For the given problem, the critical pressure is observed to take place at Mode 2 which corresponds to a buckling pressure of 57.8 MPa.

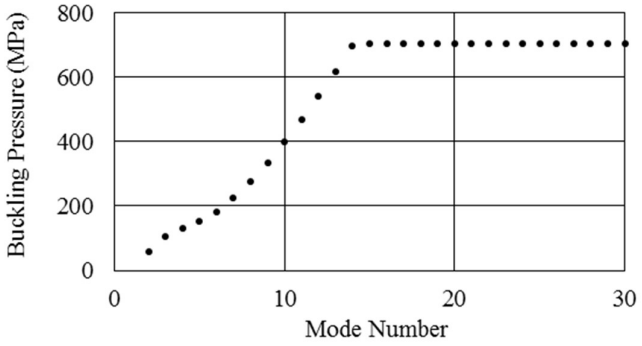

Figure 6. Buckling pressure for modes n = 2,3,…30

7.3.3 Comparison of Buckling Pressure and Mode Shapes

Throughout buckling, the system undergoes both radial and tangential displacements. The displacements are the functions of the r and θ. Based on the displacement functions in Eq. (12), Figure 7 shows a comparison between the present study and Abaqus. Figure 7 (a) shows the radial displacement in terms of r when $\theta = 0$ and Figure 7 (b) shows the tangential displacement in terms of r when $\theta = \pi/4$. Table 3 compares the buckling pressures of the system for first five buckling modes. The governing buckling pressure, which corresponds to the second mode, agrees with the Abaqus model within 1.7 %. Larger differences are observed between both models are observed for higher modes. This is the case because of two reasons: (a) while the present solution accounts for the follower effect, the ABAQUS solution is unable to capture the follower effect in an Eigenvalue analysis (Simulia, 2011), (b) as reported in Ji and Waas (2012) and (2013) and in Ji et al (2010) and (2013) the stress-strain-constitutive measures adopted in ABAQUS (based on the Jaumann rate of the Kirchhoff stress tensor), and the Green-Lagrange Strain tensor with a constant constitutive moduli are work-conjugate only in an approximate sense. In contrast, the present study adopts the Cauchy stress tensor, the Green-Lagrange Strain tensor, and constant constitutive moduli are energy conjugate. For thick homogeneous pipes, Ji and Waas (2013) have numerically shown that the error involved by adopting non-conjugate stress-strain-constitutive triplets in ABAQUS leads to an overestimation of the critical pressure. A similar observation is observed in the present study for the case of sandwich pipes.

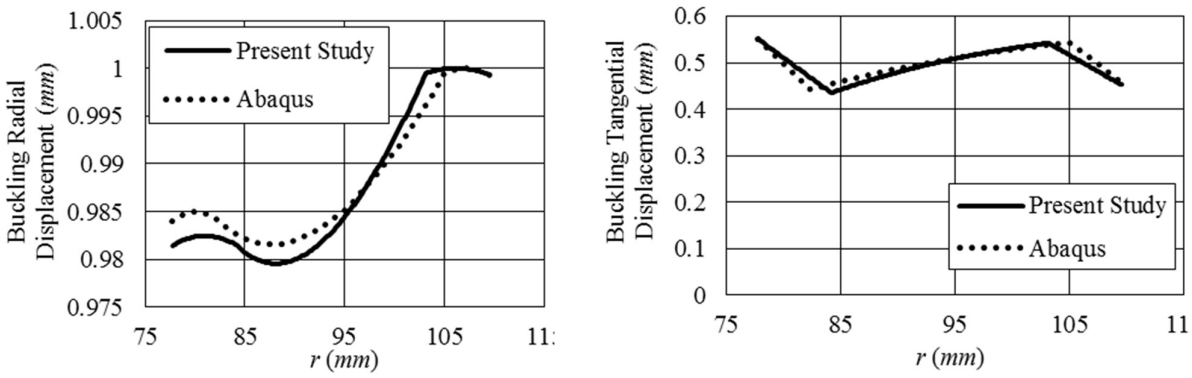

(a) (b)

Figure 7 (a) radial buckling displacements for $\theta = 0$ (b) tangential buckling displacement for $\theta = \pi/4$

Table 1. Buckling Configuration of different Modes

Mode	$n = 2$	$n = 3$	$n = 4$	$n = 5$	$n = 6$
FD Solution					
P_{cr} (MPa)	58	105	130	152	183
Abaqus	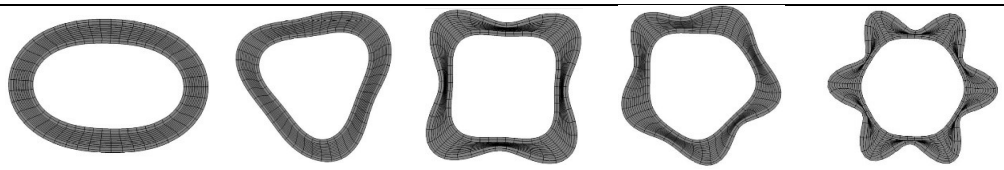				
P_{cr} (MPa)	59	113	138	177	195

7.4 Effect of shear deformation:

In order to assess the effect of shear deformation, the present solution is compared to that of the non-shear deformable solution in Kyriakides and Corona (2007). **Error! Reference source not found.** (a) depicts the normalized buckling pressure normalized with respect the modulus of elasticity for a single steel pipe (E_s =200,000 MPa, $\upsilon_s = 0.3$) Both solutions agree well for relatively thin pipes suggesting that the effect of shear deformation is minor in thin pipes. For thicker pipes, the effect of shear deformation becomes pronounced as evidenced by the large difference between both solutions.

The results suggests that for steel pipes with common sizes, shear deformation effects are negligible. However, for the core where the diameter to thickness ratio is large, such effects gain significance.

7.5 Effect of Core Material

Different combinations Poisson ratio υ_c values are considered for the core layer to investigate its effect on the buckling pressure of sandwich pipe system. Figure 8 (b) shows that an increase in the Poisson ratio has a negligible effect on the buckling pressure.

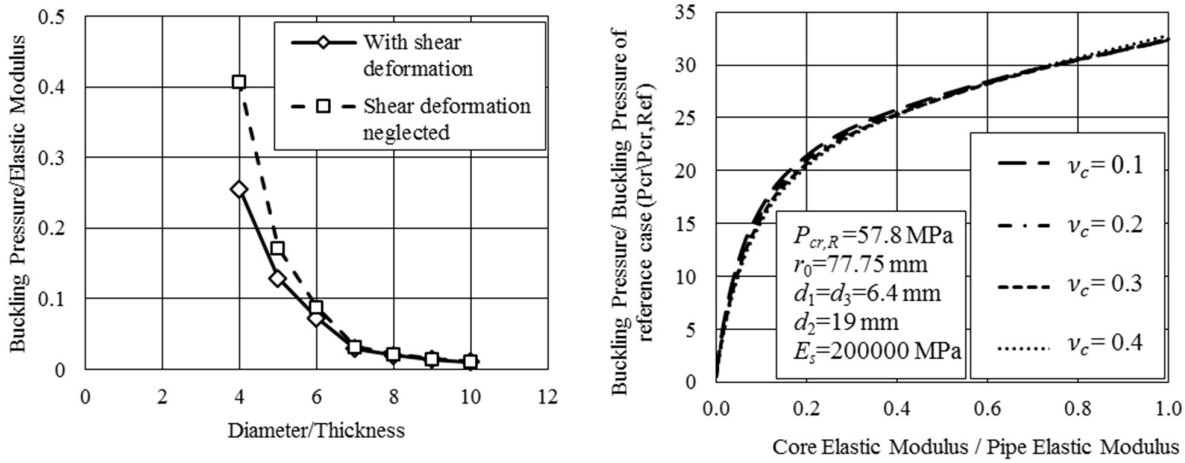

(a) (b)

Figure 8. Sensitivity analysis (a) effect of diameter to thickness, and (b) Effect of Poisson ratio of the core

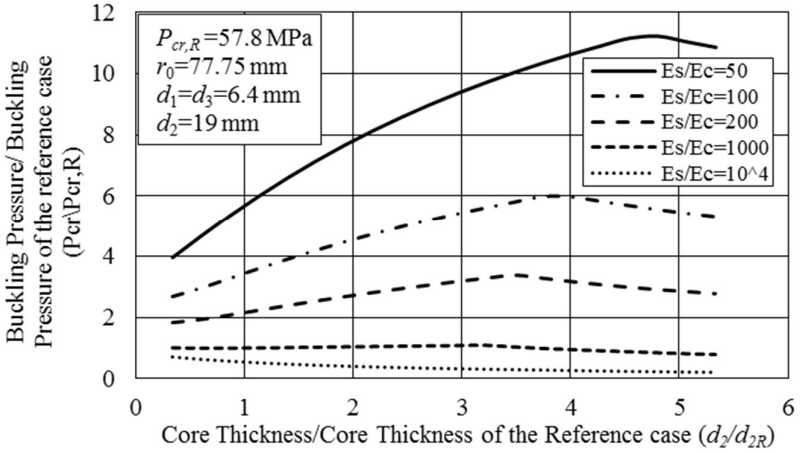

Figure 9. Normalized buckling pressure as a function of core thickness

7.6 Effect of Core Thickness

The effect of the core thickness on the buckling pressure of the system is assessed by keeping the internal radius constant while varying the external radius to change the core thickness. Five different scenarios with E_s/E_c = 50, 100, 200, 10^3, and 10^4 were considered while all other properties were kept constant and equal to those based on the reference case. The results are shown in Figure 9. It shows that when the core is soft compared to the steel (e.g., E_s/E_c=10^4), increasing the core thickness is found to reduce the buckling capacity of the system. However, when the core is stiff (e.g., E_s/E_c=200), the buckling capacity of the system is observed to increase with the core thickness until it reaches a peak value after which the capacity starts to decrease. As the core becomes stiffer (i.e., E_s/E_c is smaller), the normalized core thickness d_2/d_{2R} at which the peak buckling pressure takes place, becomes larger.

7.7 External and Internal Pipe Thicknesses

The effect of the thickness of internal and external pipes on the buckling capacity of the sandwich pipe system is investigated in this section. A range of thickness ratios (0.3 to 3.1) relative to the reference case is considered both for the internal and external pipes. For each case, a buckling analysis was conducted for various buckling modes. When the external pipe thickness is considerably smaller than that of the internal pipe (e.g. $t_{ext} = 4\,mm$ and $t_{int} = 12\,mm$), the system tends to buckle in a higher mode (in this case n = 6). Figure 10 shows the buckling capacity of the system for first 11 modes. Figure 11 shows the effect of internal and external pipe thicknesses on the normalized buckling capacity. It is observed that increasing both pipe thicknesses corresponds to an increase in the

buckling capacity. Increasing the external pipe thickness is observed to be more effective in increasing the normalized pressure compared to increasing the internal pipe thickness.

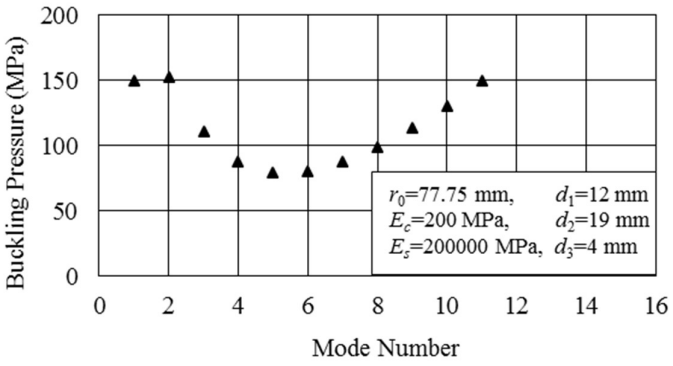

Figure 10. Buckling pressure of a sandwich pipe system in higher mode

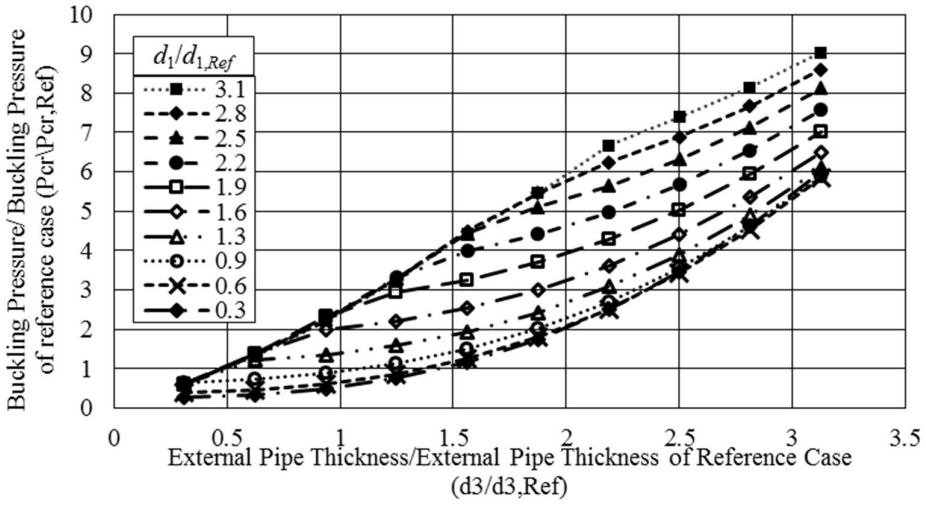

Figure 11. Normalized buckling pressure of the sandwich pipe versus the normalized thickness of the external pipe

8 Simpilified Solution

The present section aims at developing a simplified equation to predict the critical external pressure. Considering that the buckling capacity of a sandwich pipe system is a function of the radii and

thicknesses of the there layers as well as their material properties, one can express the normalized critical pressure of the system as a function of six dimenssionless parameters

$$\frac{P_{cr}}{P_{cr,ext}} = \overline{F}_1\left(\frac{R_{int}}{R_{ext}}, \frac{R_{int}}{t_{int}}, \frac{R_{ext}}{t_{ext}}, \frac{E_c}{E_s}, \upsilon_c, \upsilon_s\right) \tag{31}$$

where $P_{cr,ext}$, the buckling capacity of the external pipe, has been used as a reference against which the critical pressure of the sandwich system is normalized.

8.1 Parametric Runs

A set of parametric runs was conducted to assess the effect of the Poisson ratio of the core, and the ratios of internal thickness to internal radius, external thickness to external radius, and internal radius to external radius. The results are depicted Figure 12 (a) - (d).

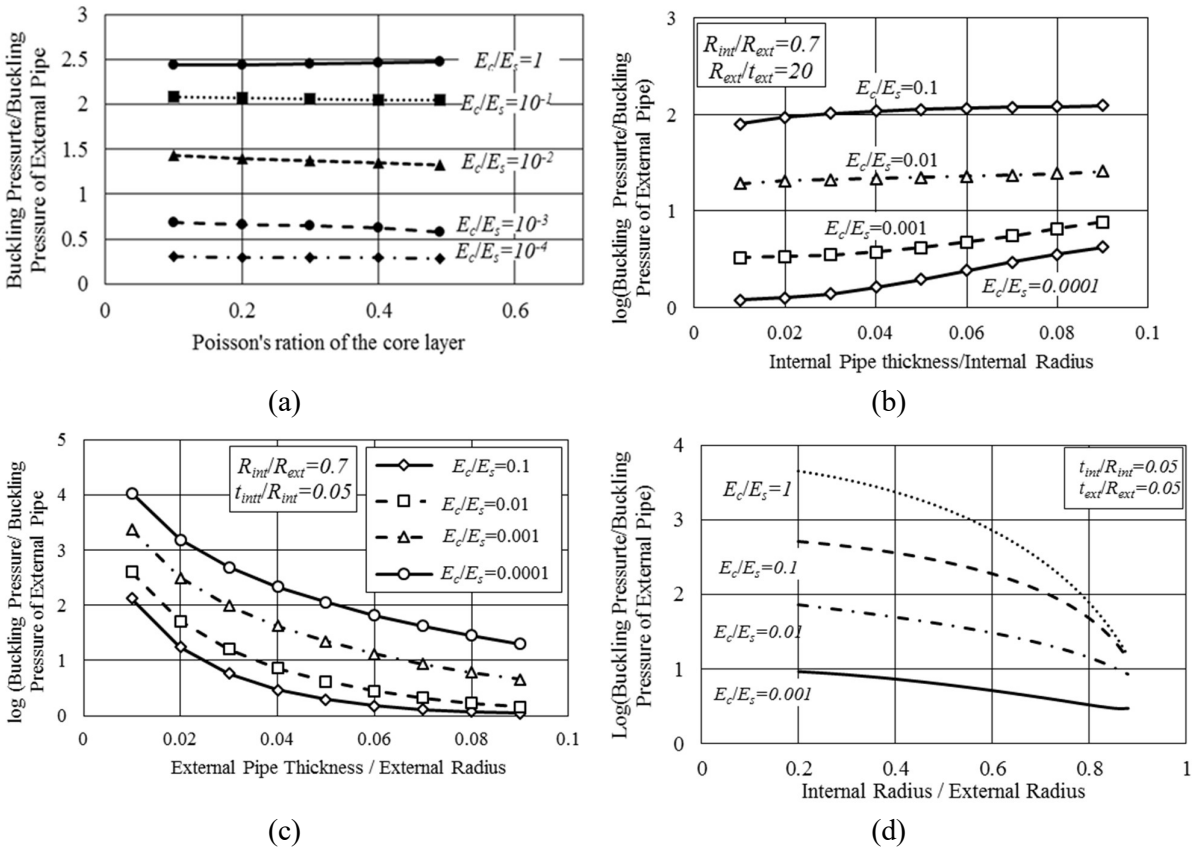

Figure 12. Effects of various parameter on the buckling pressure ratio (a) Poisson's ratio of the core, (b) internal thickness to internal thickness ratio (t_{int}/R_{int}), (c) external thickness to external radius ratio (t_{ext}/R_{ext}), and (d) internal radius to external radius ratio (R_{int}/R_{ext}),

Figure 12 (a) demonstrates that, irrespective of the modulus of elasticity of the core E_c/E_s, its Poisson's ratio υ_c has a negligible influence of the buckling capacity of the system. It is thus reasoned that this parameter can be omitted from the regression expression. Figure 12 (b) indicates that the effect of internal thickness to internal thickness ratio (t_{int}/R_{int}) has a minor effect. In contrast, Figure 12 (c,d) suggest that parameters tint/R_{int} and t_{ext}/R_{ext} have a significant effect on the buckling capacity of the system. All four figures indicate that the effect of the core to steel modular ratio E_c/E_s is rather significant. The above observations lead to a reduction of the number of influential parameters and one can re-write Eq. (31) as a function of four parameters without much loss in accuracy.

$$\frac{P_{cr}}{P_{cr,ext}} \approx \overline{F}_2\left(\frac{R_{ext}}{t_{ext}}, \frac{E_c}{E_s}, \frac{R_{int}}{t_{int}}, \frac{R_{int}}{R_{ext}}\right) \tag{32}$$

A total of 900 runs were conducted to cover the practical range of the parameters in the right hand side of Eq. (32): The radius to thickness ratios R_{ext}/t_{ext} and R_{int}/t_{int} were varied between 10 to 50 the modular ratios E_c/E_s were varied between 10^{-5} and 10^{-1} while R_{int}/R_{ext} were varied between 0.5 and 0.8. Four equations of the form $\left(P_{cr}/P_{cr,ext}\right)_i \approx F_i\left(R_{ext}/t_{ext}, E_c/E_s, R_{int}/t_{int}\right)$ were fitted for the cases $\left(R_{int}/R_{ext}\right)_i = 0.5, 0.6, 0.7,$ and 0.8. Critical pressures for intermediate R_{int}/R_{ext} values can be obtained by linear interpolation. Functions of the form

$$Y_i = \left(C_{0i} + C_{1i}X_1 + C_{2i}X_2 + C_{3i}X_1^2 + C_{4i}X_1X_2 + C_{5i}X_2^2 + C_{6i}X_1^2X_2 + C_{7i}X_1X_2^2\right)\left(1 + C_{8i}X_3^2\right) \tag{33}$$

were fitted to the results of the 900 runs conducted where $Y_i = \log\left(P_{cr}/P_{cr,ext}\right)_i$, $X_1 = R_{ext}/t_{ext}$, $X_2 = \log\left(E_c/E_s\right)$, and $X_3 = R_{int}/t_{int}$. The regression coefficients $C_{0i-8i}, i = 1,2,3,4$ are provided in

Table 2 and a comparison between predictions of the regression equations in (Eq. 33) and those based on the present FD model are provided in Figure 13 for a sample of the runs conducted.

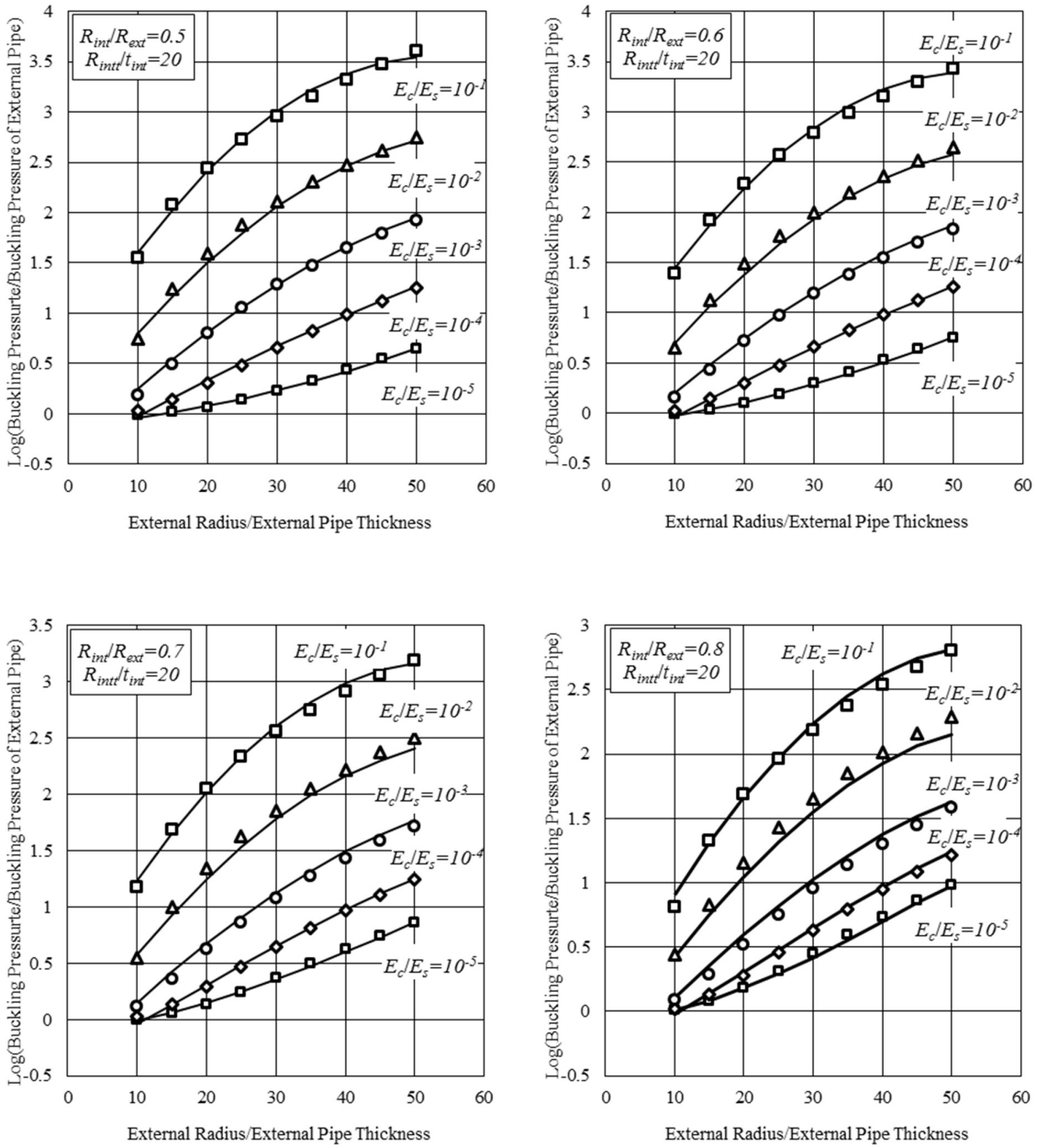

Figure 13. Comparison of buckling pressure predictions based on regression (denoted by symbols) and those based on finite difference model (solid lines)

Table 2. Regression coefficients of the simplified equations

i	$\frac{R_{int}}{R_{ext}}$	Regression coefficients								
		C_{0i}	C_{1i}	C_{2i}	C_{3i}	C_{4i}	C_{5i}	C_{6i}	C_{7i}	C_{8i}
1	0.5	1.1052	0.09348	0.8086	-1.02E-03	8.99E-03	0.1142	-2.31E-04	-1.77E-03	149.6
2	0.6	0.9437	0.09333	0.7361	-9.98E-04	1.09E-02	0.1066	-2.39E-04	-1.41E-03	149.6
3	0.7	0.7096	0.09246	0.6215	-9.59E-04	1.30E-02	9.35E-02	-2.44E-04	-9.71E-04	149.6
4	0.8	0.3166	0.09043	0.4073	-8.93E-04	1.57E-02	6.67E-02	-2.47E-04	-3.82E-04	149.6

8.2 Assessment of Effect of Interpolation

Functions $Y_i (i = 1,2,3,4)$ proposed in Eq. 32 provide the external pressure ratios at the specific values $\left(R_{int}/R_{ext}\right)_i = 0.5, 0.6, 0.7,$ and 0.8. When $\left(R_{int}/R_{ext}\right)$ takes intermediate values, linear interpolation is proposed. To assess the effect of interpolation on the predicted critical pressure, the case $\left(R_{int}/R_{ext}\right) = 0.65$ is considered. Two cases were considered for $t_{int}/R_{int} = 0.04, 0.06$ where E_c/E_s=10^{-4} and $\upsilon_c = 0.15$. The critical pressure ratio was obtained by averaging the predictions of Y_2 (for $R_{int}/R_{ext} = 0.60$) and Y_3 (for $R_{int}/R_{ext} = 0.70$) yielding the solid and dotted lines in Figure 14. Results were also obtained from the finite difference model for comparison. The results indicate that the error induced by interpolation is minimal and is are able to reasonably replicate the critical pressures predicted by the finite difference model.

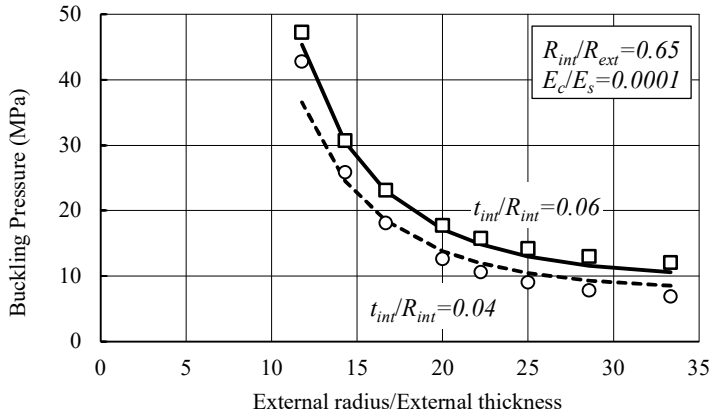

Figure 14. Comparison between the simplified solution with interpolation (solid and dotted lines) and the finite difference solution (symbols)

9 Summary

The principle of stationary potential energy was used to formulate a closed-form solution for the pre-buckling equilibrium conditions and boundary conditions for multi-layer sandwich pipe systems. The governing neutral stability conditions and associated boundary conditions throughout buckling were also formulated. A Fourier series expansion of the displacement fields was adopted and was found to be particularly useful in transforming the 2D problem into a series of 1D independent problems, thus preserving the accuracy of the solution while keeping the degrees of freedom involved to a minimum. The resulting equations were discretized using the finite difference technique. A verification study was conducted through comparison with Abaqus solutions, and the validity of the formulation was established. The formulation features the following aspects:

1. It accounts for shear deformation effects and is thus suited for composite pipe systems with thick cores.
2. It involves two destabilizing terms: one is due to the external hydrostatic pressure and incorporates the follower effects, and the other one is due to the pre-bucking stresses

undergoing the nonlinear components of the strains. The second contribution has been neglected in most published studies on sandwich pipes.

3. It adopts the Cauchy stress tensor and Green-Lagrange strain tensor with constant constitutive relation as a work conjugate stress-strain-constitutive relation, which are energy-conjugate triplets, and thus is judged to provide a superior solution compared to most commercial software (Fu and Wass 2014), in which energy conjugacy is achieved only in an approximate sense.
4. A simplified design equation was developed for the prediction of the critical pressure based on key geometric and material parameters.

10 Conclusions and Recommendations

Based on the parametric runs in the present study, the following conclusions can be drawn:

1. When the internal pipe is considerably thicker than the external pipe, the system tends to buckle in higher modes.
2. The elastic modulus of the core has the most influence on the buckling capacity of the system. An increase in the Elasticity Modulus of the core material significantly increases the buckling capacity of the system. In contrast, an increase in Poisson's ratio for the core was observed to only mildly decrease the buckling capacity of the sandwich system.
3. In general, increasing the internal and external pipe thickness improves the buckling capacity of the system. In most cases, external pipe thickness is observed to be more influential on buckling pressure of the system.
4. For sandwich systems with soft core, the buckling capacity of the system decreases as the core thickness increases. Conversely, in sandwich systems with stiff cores, increasing the core thickness increases the buckling capacity until a maximum critical pressure value is reached.

Further increases in core thickness beyond this point are associated with a decrease in the sandwich system capacity.

5. It is recommended to expand the study to incorporate the effect of initial imperfections. Unlike the present solution, such an expansion will result in coupling between various modes and will transform the eigen value solution into a geomertically nonlinear incremental analysis.

Acknowledgments

The authors gratefully acknowledge funding from the Natural Sciences and Engineering Research Council (NSERC) of Canada to the second author.

11 Appendices

11.1 Appendix A

The total strains defined in Eqs. 3 are composed of four types of terms: pre-buckling linear, buckling non-linear, buckling linear, and buckling nonlinear strains. In the following, each category is rewritten based on the associated pre-buckling or buckling displacement. The linear pre-buckling strains at Configuration (d) are:

$$\varepsilon^{j}_{r,L,p} = u'^{j}_{pI} + \lambda u'^{j}_{pE} \quad \text{A.1}$$

$$\varepsilon^{j}_{\theta,L,p} = (1/r)\left(u'^{j}_{pI} + \lambda u'^{j}_{pE}\right) \quad \text{A.2}$$

$$\gamma^{j}_{r\theta,L,p} = 0 \quad \text{A.3}$$

The non-linear pre-buckling strains are

$$\varepsilon^{j}_{r,NL,p} = 1/2\left(u'^{j}_{pI} + \lambda u'^{j}_{pE}\right)^2 \quad \text{A.4}$$

$$\varepsilon^{j}_{\theta,NL,p} = \left(1/2r^2\right)\left(u^{j}_{pI} + \lambda u^{j}_{pE}\right)^2 \quad \text{A.5}$$

$$\gamma^{j}_{r\theta,NL,p} = 0 \quad \text{A.6}$$

The buckling strains have been defined as those based on Configuration (e) after subtracting those at Configuration (d). The linear buckling strains are:

$$\varepsilon^j_{r,L,b} = u'^j_b \qquad \text{A.7}$$

$$\varepsilon^j_{\theta,L,b} = (1/r)\left(u^j_b + \dot{v}^j_b\right) \qquad \text{A.8}$$

$$\gamma^j_{r\theta,L,b} = (1/r)\left(\dot{u}^j_b - v^j_b\right) + v'^j_b \qquad \text{A.9}$$

And the non-linear buckling strains are;

$$\varepsilon^j_{r,NL,b} = 1/2\left[u'^{j2}_b + v'^{j2}_b + 2\left(u'^j_{pI} + \lambda u'^j_{pE}\right)u'^j_b\right] \qquad \text{A.10}$$

$$\varepsilon^j_{\theta,NL,b} = \left(1/2r^2\right)\left[\dot{u}^{j2}_b + v^{j2}_b - 2\dot{u}^j_b v^j_b + u^{j2}_b + \dot{v}^{j2}_b + 2\left(u^j_{pI} + \lambda u^j_{pE}\right)u^j_b + 2\left(u^j_{pI} + \lambda u^j_{pE} + u^j_b\right)\dot{v}^j_b\right] \qquad \text{A.11}$$

$$\gamma^j_{r\theta,NL,b} = (1/r)\left[\dot{u}^j_b\left(u'^j_{pI} + \lambda u'^j_{pE} + u'^j_b\right) - \left(u'^j_{pI} + \lambda u'^j_{pE} + u'^j_b\right)v^j_b + \left(u^j_{pI} + \lambda u^j_{pE} + u^j_b\right)v'^j_b + v'^j_b\dot{v}^j_b\right] \qquad \text{A.12}$$

11.2 Appendix B

This appendix provides the coefficients $A^j_{k,m}\left(k=1,2, m=1,...6\right)$ and $B^j_{k,m}\left(k=1,2, m=1,...5\right)$ introduced in the neutral stability conditions (Eqs. 15 and 16) as well as $C^j_{k,m}\left(k=1,...4, m=1,2,3\right)$ and $D^j_{k,m}\left(k=1,...4, m=1,2,3\right)$ introduced in the boundary conditions (Eqs. 17 to 22). In general, the coefficients depend on the radius, Poisson's ratio, pre-buckling displacements and Lame's constant

$$A^j_{1,1} = +\left(1-\upsilon^j\right)/r \qquad A^j_{2,1} = -(3-4\upsilon^j)/(2r)$$

$$A^j_{1,2} = -\left(1-\upsilon^j\right) \qquad A^j_{2,2} = -1/2$$

$$A^j_{1,3} = -r\left(1-\upsilon^j\right) \qquad A^j_{2,3} = +\left(1-2\upsilon^j\right)/(2r)$$

$$A^j_{1,4} = -\left(1-2\upsilon^j\right)/(2r) \qquad A^j_{2,4} = -\left(1-2\upsilon^j\right)/2$$

$$A_{1,5}^{j} = +(3-4\upsilon^{j})/(2r) \qquad A_{2,5}^{j} = -r\left(1-2\upsilon^{j}\right)/2$$

$$A_{1,6}^{j} = -1/2 \qquad A_{2,6}^{j} = -\left(1-\upsilon^{j}\right)/r$$

$$B_{1,1}^{j} = \left(1-\upsilon^{j}\right)u_{pE}^{j}/r^{2} + \upsilon^{j}u_{pE}^{\prime j}/r \qquad B_{2,1}^{j} = -2\left(1-\upsilon^{j}\right)u_{pE}^{j}/r^{2} - 2\upsilon^{j}u_{pE}^{\prime j}/r$$

$$B_{1,2}^{j} = -u_{pE}^{\prime j} - \left(1-\upsilon^{j}\right)ru_{pE}^{\prime\prime j} \qquad B_{2,2}^{j} = +\left(1-\upsilon^{j}\right)u_{pE}^{j}/r^{2} + \upsilon^{j}u_{pE}^{\prime j}/r$$

$$B_{1,3}^{j} = -\upsilon^{j}u_{pE}^{j} - \left(1-\upsilon^{j}\right)ru_{pE}^{\prime j} \qquad B_{2,3}^{j} = -u_{pE}^{\prime j} - r\left(1-\upsilon^{j}\right)u_{pE}^{\prime\prime j}$$

$$B_{1,4}^{j} = -\left(1-\upsilon^{j}\right)u_{pE}^{j}/r^{2} - \upsilon^{j}u_{pE}^{\prime j}/r \qquad B_{2,4}^{j} = -\upsilon^{j}u_{pE}^{j} - r\left(1-\upsilon^{j}\right)u_{pE}^{\prime j}$$

$$B_{1,5}^{j} = 2\left(1-\upsilon^{j}\right)u_{pE}^{j}/r^{2} + 2\upsilon^{j}u_{pE}^{\prime j}/r \qquad B_{2,5}^{j} = -\left(1-\upsilon^{j}\right)u_{pE}^{j}/r^{2} - \upsilon^{j}u_{pE}^{\prime j}/r$$

$$C_{1,1}^{j} = \begin{cases} L^{j} & (\text{for } j \neq 1) \\ L^{j} + P_{int} & (\text{for } j = 1) \end{cases} \qquad C_{2,1}^{j} = \begin{cases} L^{j}\left(1-2\upsilon^{j}\right)/(2\upsilon^{j}) & (\text{for } j \neq 1) \\ L^{j}\left(1-2\upsilon^{j}\right)/(2\upsilon^{j}) - P_{int} & (\text{for } j = 1) \end{cases}$$

$$C_{1,2}^{j} = L^{j}\left(1-\upsilon^{j}\right)r_{j-1}/\upsilon^{j} \qquad C_{2,2}^{j} \in \begin{cases} -L^{j}\left(1-2\upsilon^{j}\right)/(2\upsilon^{j}) & (\text{ for } j \neq 1) \\ -L^{j}\left(1-2\upsilon^{j}\right)/(2\upsilon^{j}) + P_{int} & (\text{ for } j = 1) \end{cases}$$

$$C_{1,3}^{j} = \begin{cases} L^{j} & (\text{for } j \neq 1) \\ L^{j} + P_{int} & (\text{for } j = 1) \end{cases} \qquad C_{2,3}^{j} = L^{j}\left(1-2\upsilon^{j}\right)r_{j-1}/(2\upsilon^{j})$$

$$D_{1,1}^{j} = L^{j}u_{pE}^{j} + L^{j}\left(1-\upsilon^{j}\right)r_{j-1}u_{pE}^{\prime j}/\upsilon^{j} \qquad D_{2,1}^{j} = L^{j}u_{pE}^{j} + L^{j}\left(1-\upsilon^{j}\right)r_{j-1}u_{pE}^{\prime j}/\upsilon^{j}$$

$$C_{3,1}^{j} = L^{j} \qquad C_{4,1}^{j} = L^{j}\left(1-2\upsilon^{j}\right)/(2\upsilon^{j})$$

$$C_{3,2}^{j} = L^{j}\left(1-\upsilon^{j}\right)r_{j}/\upsilon^{j} \qquad C_{4,2}^{j} = -L^{j}\left(1-2\upsilon^{j}\right)/(2\upsilon^{j})$$

$$C_{3,3}^{j} = L^{j} \qquad C_{4,3}^{j} = L^{j}\left(1-2\upsilon^{j}\right)r_{j}/(2\upsilon^{j})$$

$$D_{3,1}^{j} = \begin{cases} 0 & (\text{for } j \neq l) \\ P_{ext} & (\text{for } j = l) \end{cases} \qquad D_{4,1}^{j} = \begin{cases} 0 & (\text{for } j \neq l) \\ -P_{ext} & (\text{for } j = l) \end{cases}$$

$$D_{3,2}^{j} = L^{j}u_{pE}^{j} + L^{j}\left(1-\upsilon^{j}\right)r_{j}u_{pE}^{\prime j}/\upsilon^{j} \qquad D_{4,2}^{j} = \begin{cases} 0 & (\text{for } j \neq l) \\ P_{ext} & (\text{for } j = l) \end{cases}$$

$$D_{3,3}^{j}=\begin{cases}0 & \left(\text{for } j\neq l\right)\\ P_{ext} & \left(\text{for } j=l\right)\end{cases} \qquad D_{4,3}^{j}=L^{j}u_{pE}^{j}+L^{j}\left(1-\upsilon^{j}\right)r_{j}u_{pE}^{\prime j}\Big/\upsilon^{j}$$

12 References

Arjomandi, K., Taheri, F., 2010. Elastic buckling capacity of bonded and unbonded sandwich pipes under external hydrostatic pressure. Journal of Mechanics of Materials and Structures 5 (3), 391-409.

Arjomandi, K., Taheri, F., 2011. Stability and post-buckling response of sandwich pipes under hydrostatic external pressure. International Journal of Pressure Vessels and Piping 88 (4), 138-148.

Brush, D.O., Almroth, B.O., 1975. Buckling of bars, plates, and shells. McGraw-Hill, New York.

Castello, X., Estefen, S.F., 2006. Adhesion Effect On The Ultimate Strength Of Sandwich Pipes, 25th International Conference on Offshore Mechanics and Arctic Engineering. ASME, Hamburg, Germany, pp. 261-267.

Fu, G., Moura Paz, C., Chujutalli., J.A.H., Lourenço., M.I., Jr., D.B.d.L., Li., Y., Filho., R.T., Estefen., S.F., 2014. Sandwich Pipes With Strain Hardening Cementitious Composites (Shcc). Numerical Analyses, 33rd International Conference on Ocean, Offshore and Arctic Engineering. ASME, San Francisco, California, USA, pp.V06AT04A030.

Fu, L., Waas, A.M., 1995. Initial post-buckling behavior of thick rings under uniform external hydrostatic pressure. Journal of Applied Mechanics 62 (2), 338-345.

Hashemian, R., 2014. Buckling Analysis Of Sandwich Pipes Under External Pressure, Faculty of Graduate and Postdoctoral Studies. University of Ottawa, Ottawa, Canada.

Ji, W., Waas, A.M., 2012. Accurate buckling load calculations of a thick orthotropic sandwich panel. Composites Science and Technology 72 (10), 1134-1139.

Ji, W., Waas, A.M., 2013. The Two-Dimensional Elasticity Solution for the Buckling of a Thick Orthotropic Ring Under External Pressure Loading. Journal of Applied Mechanics 81 (1), 011005-011005.

Ji, W., Waas, A.M., Bazant, Z.P., 2013. On the Importance of Work-Conjugacy and Objective Stress Rates in Finite Deformation Incremental Finite Element Analysis. Journal of Applied Mechanics 80 (4), 041024-041024.

Ji, W., Waas, A.M., Bažant, Z.P., 2010. Errors Caused by Non-Work-Conjugate Stress and Strain Measures and Necessary Corrections in Finite Element Programs. Journal of Applied Mechanics 77 (4), 044504-044504.

Kardomateas, G.A., 1993. Buckling of thick orthotropic cylindrical shells under external pressure. Journal of Applied Mechanics 60 (1), 195-202.

Kardomateas, G.A., Simitses, G.J., 2004. Buckling of long sandwich cylindrical shells under external pressure. Journal of Applied Mechanics 72 (4), 493-499.

Papadakis, G., 2008. Buckling of thick cylindrical shells under external pressure: A new analytical expression for the critical load and comparison with elasticity solutions. International Journal of Solids and Structures 45 (20), 5308-5321.

Sato, M., Patel, M.H., 2007. Exact and simplified estimations for elastic buckling pressures of structural pipe-in-pipe cross sections under external hydrostatic pressure. Journal of Marine Science and Technology 12 (4), 251-262.

Simulia, 2011. Abaqus 6.11 Online Documentation. Dassault Systèmes, RI, USA.